Energy and Buildings 94 (2015) 21–32

Contents lists available at ScienceDirect

Energy and Buildings

journal homepage: www.elsevier.com/locate/enbuild

Development and optimization of an innovative HVAC system with integrated PVT and PCM thermal storage for a net-zero energy retrofitted house

Massimo Fiorentini*, Paul Cooper, Zhenjun Ma

Sustainable Buildings Research Centre (SBRC), Faculty of Engineering and Information Sciences, University of Wollongong, Innovation Campus, Building 237, Squires Way, North Wollongong 2522, NSW, Australia

ARTICLE INFO

Article history:
Received 19 December 2014
Accepted 7 February 2015
Available online 25 February 2015

Keywords:
Solar-assisted HVAC system
Photovoltaic–thermal
Phase change material
Thermal modelling
Experimental validation

ABSTRACT

This paper describes a novel solar-assisted HVAC system developed for the Team UOW 'Illawarra Flame' Solar Decathlon house, the winner of the Solar Decathlon China 2013 competition. This HVAC system consists of an air-based photovoltaic–thermal (PVT) collector and a phase change material (PCM) thermal storage unit integrated with a reverse cycle heat pump, in a ducted system. The system was designed for operation during both winter and summer using daytime solar radiation and night-time sky radiative cooling, respectively. The PVT collector heats or cools fresh air from ambient and thereby provides heating or cooling either directly to the indoor space, or to the PCM storage unit. The heat stored in the PCM can be used later to condition the space or precondition the air entering the air handling unit. Analytical models for the PVT collector and PCM unit were developed in order to be easily implemented into a practical building management system (BMS). Experimental studies on the PVT collector and PCM unit were carried out and the data was used to validate the effectiveness of the models. It is shown that there is a good agreement between the model simulation results and experimental test data. A simple optimisation methodology of the operating modes that involve these components is also presented.

© 2015 Elsevier B.V. All rights reserved.

1. Introduction

Every year only approximately 1 to 2% of the Australian residential building stock is replaced by or added to by new buildings [1]. Many of the houses built in Australia after the Second World War were timber-framed houses, clad in fibre-cement and were hence colloquially named 'fibro' houses. These buildings typically have little or no thermal insulation and generally exhibit poor thermal performance and low energy efficiency. Under the auspices of the University of Wollongong (UOW) Sustainable Buildings Research Centre (SBRC) a student/staff team (Team UOW) was formed with the members drawn from both the University of Wollongong and TAFE (Technical and Further Education) NSW (New South Wales) Illawarra Institute. Team UOW set out to be the first team in the history of Solar Decathlon competitions to demonstrate how to effectively upgrade and retrofit an existing building rather than designing a new building from scratch. This approach proved to be extremely successful and Team UOW subsequently won the Solar Decathlon China 2013 competition with the highest overall score in the history of Solar Decathlon competitions, which have run in the USA, Europe and China since 2002. Team UOW decided to develop a retrofitting strategy to demonstrate how to improve the level of thermal comfort and overall sustainability performance of a 'fibro' home through the development and application of different retrofit technologies. One of the key targets was to achieve net-zero energy consumption in that the grid-connected building was to generate more renewable energy on-site than that it imports from the grid over the course of a year. To achieve this target, it is first necessary to reduce the energy demand of the building through the implementation of effective passive retrofitting initiatives, such as upgrading the envelope, glazing and shading systems, using natural ventilation, etc. followed retrofitting and application of advanced active systems.

The development and implementation of an innovative HVAC system incorporating advanced sustainable energy technologies was a desired outcome of the project. Solar photovoltaic–thermal (PVT) collectors were seen as a promising technology that was receiving wide attention. Cooling of the PV modules by the heat transfer fluid flowing through the PVT collector then leads to an

* Corresponding author. Tel.:+610421918240.
E-mail addresses: mf877@uowmail.edu.au, maxfiore86@gmail.com (M. Fiorentini).

http://dx.doi.org/10.1016/j.enbuild.2015.02.018
0378-7788/© 2015 Elsevier B.V. All rights reserved.

Nomenclature

α	net thermal absorptivity
α_c	a weighting factor for electrical and thermal energy
A_c	cross sectional area [m^2]
β	surface slope [rad]
c_p	specific heat of air [J/kg K]
d	PVT duct depth [m]
D_h	hydraulic diameter [m]
dnr	direct normal radiation [W/m^2]
dhr	diffuse horizontal radiation [W/m^2]
doy	day of the year
η	electrical efficiency of PV panels
φ	latitude [rad]
γ	surface azimuth [rad]
ghr	global horizontal radiation [W/m^2]
$\bar{h}_{\text{in}}$	average convective heat transfer coefficient inside the duct [W/m^2 K]
$\bar{h}_{\text{in}T}$	average convective heat transfer coefficient of the bottom half inside the duct and PV panel [W/m^2 K]
h_{r1}	radiative heat transfer coefficient duct-sky [W/m^2 K]
h_{r2}	radiative heat transfer coefficient duct top plate-bottom plate [W/m^2 K]
h_{conv}	convective heat transfer coefficient between top of PV panels and air [W/m^2 K]
Ir	solar radiation on the tilted surface [W/m^2]
k	thermal conductivity of air [W/m K]
l	duct length [m]
$\dot{m}$	mass flow rate [kg/s]
Nu	Nusselt number
P	Perimeter [m]
P_{th}	heat transfer [W]
$P_{e,\text{cons}}$	fan electrical power consumption [W]
$P_{e,\text{gen}}$	increased electrical power generation [W]
ρ	air density [kg/m^3]
Re	Reynolds number
R_{PV}	R-value of PV panel, glue and steel frame [m^2 K/W]
stn	solar time number
T_{amb}	ambient temperature [°C]
$T_{\text{PCM},i}$	PCM unit inlet air temperature [°C]
$T_{\text{PCM},o}$	PCM unit outlet air temperature [°C]
T_{sky}	sky temperature [°C]
T_{space}	indoor temperature [°C]
T_{dp}	dew point temperature [°C]
T_{top}	top plate temperature [°C]
T_{bot}	bottom plate temperature [°C]
T_{PVT}	PVT outlet air temperature [°C]
u	specific internal energy [kJ/kg]
U_{int}	U-value from lower inside surface of duct to inside building [W/m^2 K]
U_{ext}	U-value from bottom surface of PV panels to ambient [W/m^2 K]
$\dot{V}$	volumetric flow rate [m^3/s]
V_w	wind speed [m/s]
ν	viscosity of air [m^2/s]
w	PVT duct width [m]
x	distance from the inlet [m]

increase in the electrical efficiency of the PV panels as compared to a conventional PV system which has higher PV cell operating temperatures. At the same time, heat transferred to or from the fluid may be used for space heating or cooling, thereby resulting in an increase in the overall energy collection and conversion efficiencies of the system.

Phase change materials (PCMs) generally have a high energy storage density and the capability to store thermal energy at a relatively constant temperature, which has been recognized as a sustainable and environmentally friendly technology to reduce building energy consumption and improve indoor thermal comfort [2,3]. Coupling PCMs with solar collectors may provide an alternative to attempting to increase the efficiency of traditional HVAC systems. Such integrated systems have been investigated since the 1970s and studies have been performed on the evaluation of the performance of air heaters coupled with PCM thermal storage units [4], determination of the thermal properties of the PCMs used [5] and sizing of the thermal storage units [6]. More recent bibliographic studies have shown that PCM thermal storage systems are a widely investigated technology and a rapidly developing research area [7,8]. PCMs have been studied over the past years in both passive and active systems [2,3] and a number of research groups have investigated PVT systems coupled with ventilated slabs for energy storage [9,10]. Studies on the effectiveness of PVT collectors during daytime heating and night-time radiative cooling have been undertaken, for both water-based and air-based systems [10–12].

This paper focusses on the development and modelling of an innovative solar PVT-assisted Heating, Ventilation and Air Conditioning (HVAC) system integrated with a PCM thermal energy storage unit. The main objective of the work described herein was to develop theoretical models which can accurately predict the heat transfer rates in an air-based PVT collector and a PCM thermal storage unit, the mechanical losses in both components, and the electrical output from the PVT collector. The model has a relatively simple structure with a low computational overhead and so that it can be easily implemented into the optimization strategies of commercial building management systems (BMSs).

2. Development of the innovative HVAC system

The Team UOW 'Illawarra Flame' Solar Decathlon house and a schematic of the HVAC developed in this project are shown in Figs. 1 and 2, respectively. The HVAC system consisted of an air-based PVT collector (shown on the left hand side of the roof in Fig. 1), a PCM thermal energy storage unit, and a standard reverse cycle air-conditioning system, using a ducted air distribution system and dampers to regulate the airflow within the system.

The use of air in the PVT collector as a working fluid was chosen to facilitate retrofitting of an existing house, with features including low maintenance requirements and the ability to integrate with conventional ducted air-conditioning systems. The PVT collector was fabricated from flexible thin-film CIGS PV panels glued to a metal flashing fixed across the 'valleys' of the roof sheeting. Air could therefore flow through the air duct between the PV panels/flashing and the roof sheeting to exchange heat with the panels.

The diurnal phase of the thermal energy generated from the PVT collector has a significant offset as compared to thermal demand of the building, for Sydney weather conditions. For this reason an active thermal storage unit was included, and a PCM has been selected as the preferred storage material. A number of types of PCMs were available on the market, each with different thermal properties and phase change temperatures, and for the present system a salt hydrate mixture with a phase change temperature of 22 °C was selected, supplied in plastic containers. To ensure the system always meet the energy demand of the house and maintain good indoor thermal comfort, a standard reverse cycle air-conditioning system with an outdoor condensing unit and an indoor air handling unit (AHU) was integrated into the system.

Fig. 1. Team UOW 'Illawarra Flame' Solar Decathlon house located at the University of Wollongong Innovation Campus.

The system was controlled by a residential control system with a programmable logic controller. This paper focuses mainly on the development and validation of the analytical models of the PVT collector and the PCM thermal storage unit and the utilisation of these models for the optimisation of the various operating modes of the HVAC system.

There are a total of five operating modes, including three conditioning modes and two PVT modes, in this HVAC system, which will be controlled through the BMS system specifically designed for this project.

2.1. Conditioning modes

Fig. 3 presents the different operating modes that the system can operate based on the indoor and outdoor measured conditions. Depending on the indoor conditions, the system can either work in natural ventilation mode through automatically controlling the opening of high level windows, or work in forced mechanical heating and cooling mode.

In the mechanical heating and cooling mode, the system can operate in three different sub-modes, as illustrated in Fig. 3a.

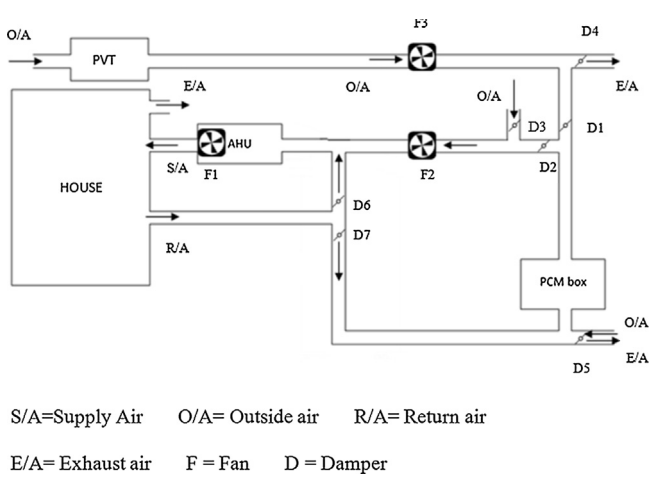

Fig. 2. Schematic of the solar-assisted HVAC system where the symbols represent the following: S/A supply air, O/A outside air, R/A return air, E/A exhaust air, F fan and D damper, respectively.

1. *Direct photovoltaic–thermal supply.* If the generation of heating during daytime or cooling during night time (night sky radiative cooling) occurs at the same time as the demand, then heated air/cooled air from the PVT system is directed into the house until the demand is matched. If the demand is higher than the energy extracted from the PVT system, the AHU will cover the remaining heating/cooling requirement.
2. *Supply air preconditioned through phase change material.* In this case, if thermal energy is available in the PCM store the mixture of return air and fresh air will be preconditioned by the PCM store, increasing or decreasing the supply air temperature. If the demand is higher than the energy extracted from the PCM storage unit, the AHU will cover the remaining heating/cooling requirement.
3. *Normal heating and cooling mode.* If there are no PVT thermal generation and no thermal energy stored in the PCM, the AHU will supply the heating or the cooling required.

2.2. PVT modes

If no interfering operating mode is activated, the system can operate in two other modes, as shown in Fig. 3b.

1. *PCM charging.* If there are no demand from the house, and the PCM unit is not fully charged as well as it is convenient to charge it, the PVT system will charge the PCM unit.
2. *PVT exhaust.* In case the increase in electrical generation of the solar panels due to their temperature decrease is higher than the energy used by the fan, the air can be drawn underneath the PV panels and exhausted directly to ambient.

3. Analytical model of the PVT collector

The PVT collector studied in this paper consisted of a number of thin-film PV panels mounted on a steel sheet 'flashing', which was fixed to the top of an existing sheet metal roof profile. This system created a cavity beneath the steel flashing through which the working fluid (i.e. air) can flow through and exchange heat with the PV panel, as shown schematically in Fig. 4.

The utilisation mode of the PVT collector generally depends on the demand of the house. For instance, when heating is required in winter daytimes, the incoming solar radiation generates

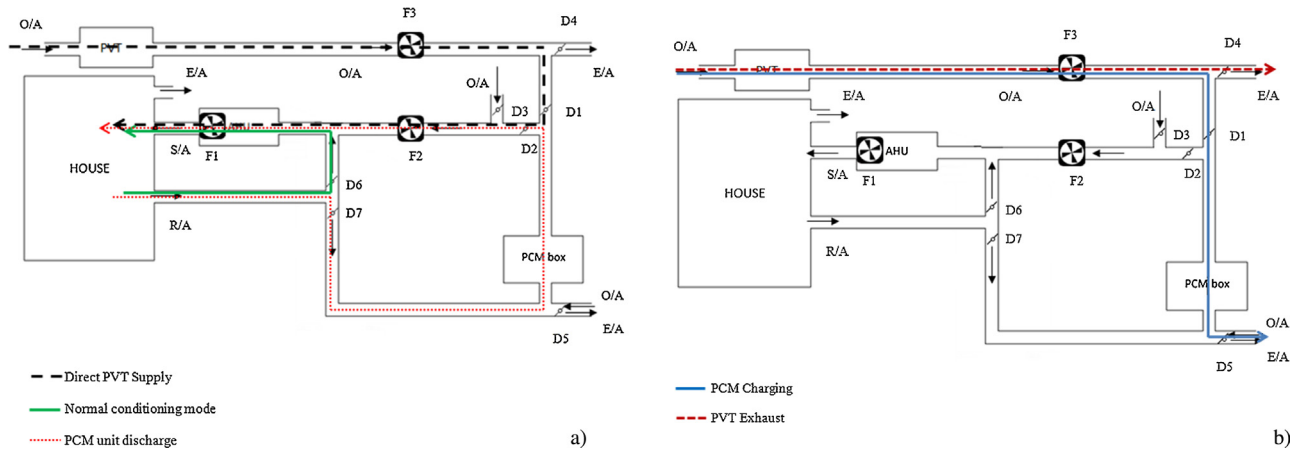

Fig. 3. Illustration of (a) HVAC system conditioning modes and (b) HVAC system PVT modes.

electricity through the PV modules. Part of the radiation is reflected/reradiated, part is lost to ambient via convection and the remainder is transferred to the heat transfer fluid (Fig. 4a). The air mass flow rate is the key parameter that allows the building management system to control the air temperature at the outlet of the PVT collector and also the quantity of heat extracted from the PV modules.

Under Sydney summer conditions the house would mainly require cooling. In this case the PVT will generate cooling during the night time, whereby the solar panels extract heat from the air flowing through the PVT collector by emitting radiation to the sky if the sky is at a lower temperature than the panels (see Fig. 4b).

So as to maximise the use of available roof space for PV electrical generation during the Solar Decathlon China 2013 competition, the PVT collector was designed so as to draw air from both the north and south elevations of the pitched roof and the two air streams then mixed in a plenum at the apex of the roof as shown in Fig. 5.

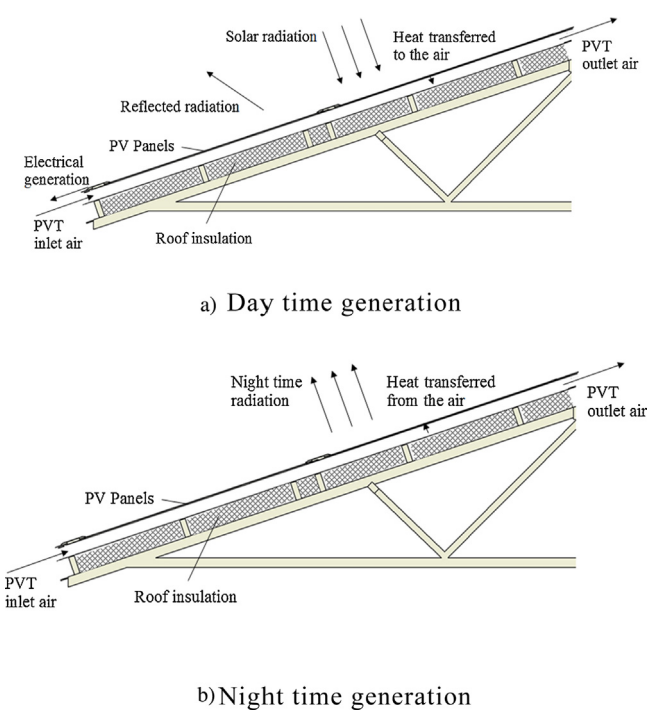

Fig. 4. Overview of the PVT collector geometry as implemented on the Illawarra Flame Solar Decathlon House.

To optimize the system and calculate the optimal airflow rate, it is necessary to accurately model the heat transfer into the air channels below the PV modules, the mechanical losses in the system, and the electrical benefit of reducing the temperature of the PV panels.

3.1. Thermal model

An analytical steady state model was developed to describe the thermal behaviour of the PVT collector. This model can be used for both design optimisation and control optimisation purposes. The key assumptions used in developing this quasi-steady state model were that: (a) the transients involved in heating or cooling of the system are relatively short compared to the time constants elsewhere in the building and HVAC system; and (b) that the conduction resistance through the upper and lower walls of the air duct are negligible in comparison to the other convection, conduction and radiation thermal resistances. These assumptions can be justified by the fact that the thin metal flashing and the thin film solar panels have relatively low thermal mass and thermal resistance (our experimental results indicated that the thermal time constant of the PVT collectors was less than five minutes).

Taking an energy balance on a short, stream-wise control volume in the PVT collector air duct, an analytical solution for the thermal performance of the collector may be derived; the thermal resistance network for heat flow at a given cross-section of the PVT collector/duct is illustrated in Fig. 6.

The energy balance on the upper and lower surfaces of the PV panel, the energy balance on the air flowing into and out of the

Fig. 5. Photovoltaic thermal (PVT) collectors implemented on the roof of the Illawarra Flame Solar Decathlon house.

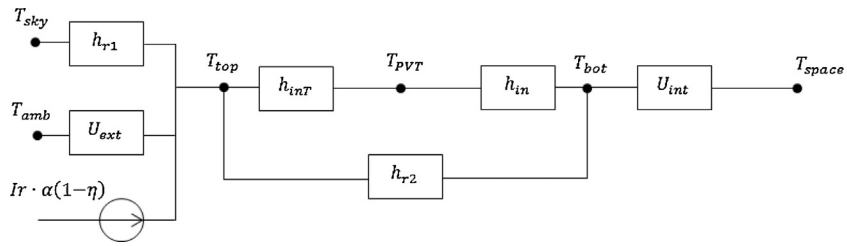

Fig. 6. Thermal resistance network model of the heat exchange at a given cross-section of the PVT collector.

control volume, and the heat balance on the lower surface of the duct may be described by (3.1), (3.2) and (3.3), respectively.

$$Ir \times \alpha(1-\eta) = U_{\text{ext}}\left(T_{\text{top}} - T_{\text{amb}}\right) + h_{r1}\left(T_{\text{top}} - T_{\text{sky}}\right) + \bar{h}_{\text{in}T}\left(T_{\text{top}} - T_{\text{PVT}}\right) + h_{r2}\left(T_{\text{top}} - T_{\text{bot}}\right) \tag{3.1}$$

$$\dot{V} \times \rho \times c_p \times \frac{\partial T_{\text{PVT}}}{\partial x}\mathrm{d}x = \left[\bar{h}_{\text{in}T}\left(T_{\text{top}} - T_{\text{PVT}}\right) + \bar{h}_{\text{in}}\left(T_{\text{bot}} - T_{\text{PVT}}\right)\right] \times w \times \mathrm{d}x \tag{3.2}$$

$$\bar{h}_{\text{in}}\left(T_{\text{PVT}} - T_{\text{bot}}\right) = U_{\text{int}}\left(T_{\text{bot}} - T_{\text{space}}\right) + h_{r2}\left(T_{\text{bot}} - T_{\text{top}}\right) \tag{3.3}$$

where $\dot{V}$ is the volumetric air flow rate, ρ and c_p are the density and specific heat capacity of the air, T_{PVT} is the local air temperature in the PVT channel, T_{top} and T_{bot} are the temperatures of the top and bottom plates of the PVT channel, $\bar{h}_{\text{in}}$ and $\bar{h}_{\text{in}T}$ are the average heat transfer coefficients on the bottom and top inside surfaces of the channel, respectively, U_{int} is the overall heat transfer coefficient between the bottom plate of the PVT channel and indoor environment, U_{ext} is the overall convective heat transfer coefficient between the top plate of the PVT channel and ambient, h_{r1} is the radiative heat transfer coefficient between the outside surface of the PV panel and the sky, h_{r2} is the radiative heat transfer coefficient between the duct top and bottom surfaces, x and w are the length and the width of the channel, respectively, T_{sky} is the temperature of the sky and T_{space} is the interior building temperature. Combining (3.1) and (3.3), the top and bottom surface temperatures of the PVT duct can be determined from (3.4) and (3.5), respectively.

$$C3 = \frac{\left(U_{\text{ext}} + \bar{h}_{\text{in}T} + h_{r1} + h_{r2}\right)\bar{h}_{\text{in}} + \bar{h}_{\text{in}T}h_{r2}}{\left(\bar{h}_{\text{in}} + h_{r2} + U_{\text{int}}\right)\left(U_{\text{ext}} + \bar{h}_{\text{in}T} + h_{r1} + h_{r2}\right) - h_{r2}^2} \tag{3.10}$$

$$C4 = \frac{\left(U_{\text{ext}} + \bar{h}_{\text{in}T} + h_{r1} + h_{r2}\right)\left(U_{\text{int}}T_{\text{space}}\right) + \text{Ir}\alpha h_{r2}(1-\eta) + U_{\text{ext}}h_{r2}T_{\text{amb}} + h_{r1}h_{r2}T_{\text{sky}}}{\left(\bar{h}_{\text{in}} + h_{r2} + U_{\text{int}}\right)\left(U_{\text{ext}} + \bar{h}_{\text{in}T} + h_{r1} + h_{r2}\right) - h_{r2}^2} \tag{3.11}$$

Combining (3.11) and (3.2) we then derive:

$$\frac{\partial T_f}{\partial x}\mathrm{d}x = \frac{w}{\dot{V} \times \rho \times c_p}\left[\left(\bar{h}_{\text{in}}C2 + \bar{h}_{\text{in}T}C4\right) + T_f\left(\bar{h}_{\text{in}T}C1 + \bar{h}_{\text{in}}C3 - \left(\bar{h}_{\text{in}} + \bar{h}_{\text{in}T}\right)\right)\right] \tag{3.12}$$

Eq. (3.12) is a first order, nonhomogeneous, linear differential equation with constant coefficients, of the form expressed in (3.13) with the general solution of (3.14).

$$y' + ay = b \qquad y = y(x) \tag{3.13}$$

$$y = \bar{y} + y^* = Ce^{-ax} + \frac{b}{a} \tag{3.14}$$

From (3.12) we can then derive (3.15):

$$\begin{cases} T'_{\text{PVT}} + AT_{\text{PVT}} = B \\ T_{\text{PVT}}(0) = T_{\text{amb}} \end{cases} \tag{3.15}$$

$$T_{\text{top}} = \frac{\left(\bar{h}_{\text{in}} + h_{r2} + U_{\text{int}}\right)\left(\left(U_{\text{ext}} + \bar{h}_{\text{in}T} + h_{r1} + h_{r2}\right)\left(T_{\text{PVT}}\bar{h}_{\text{in}} + U_{\text{int}}T_{\text{space}}\right) + Ir\,\alpha\,h_{r2}(1-\eta) + U_{\text{ext}}\,h_{r2}\,T_{\text{amb}} + T_{\text{PVT}}\,\bar{h}_{\text{in}T}\,h_{r2} + h_{r1}\,h_{r2}\,T_{\text{sky}}\right)}{h_{r2}\left(\left(\bar{h}_{\text{in}} + h_{r2} + U_{\text{int}}\right)\left(U + \bar{h}_{\text{in}T} + h_{r1} + h_{r2}\right) - {h_{r2}}^2\right)} - \frac{T_{\text{PVT}}\,\bar{h}_{\text{in}} + U_{\text{int}}\,T_{\text{space}}}{h_{r2}} \tag{3.4}$$

$$T_{\text{bot}} = \frac{\left(U_{\text{ext}} + \bar{h}_{\text{in}T} + h_{r1} + h_{r2}\right)\left(T_{\text{PVT}}\bar{h}_{\text{in}} + U_{\text{int}}T_{\text{space}}\right) + Ir\alpha h_{r2}(1-\eta) + U_{\text{ext}}\,h_{r2}\,T_{\text{amb}} + T_{\text{PVT}}\,\bar{h}_{\text{in}T}\,h_{r2} + h_{r1}\,h_{r2}\,T_{\text{sky}}}{\left(\bar{h}_{\text{in}} + h_{r2} + U_{\text{int}}\right)\left(U + \bar{h}_{\text{in}T} + h_{r1} + h_{r2}\right) - {h_{r2}}^2} \tag{3.5}$$

It is then possible to recast T_{top} and T_{bot} as follows:

$$T_{\text{top}} = C1T_{\text{PVT}} + C2 \tag{3.6}$$

$$T_{\text{bot}} = C3T_{\text{PVT}} + C4 \tag{3.7}$$

where $C1$, $C2$, $C3$ and $C4$ are coefficients and defined as follows:

$$C1 = \frac{\left(\bar{h}_{\text{in}} + h_{r2} + U_{\text{int}}\right)C3}{h_{r2}} - \frac{\bar{h}_{\text{in}}}{h_{r2}} \tag{3.8}$$

$$C2 = \frac{\left(\bar{h}_{\text{in}} + h_{r2} + U_{\text{int}}\right)C4}{h_{r2}} - \frac{U_{\text{int}}T_{\text{space}}}{h_{r2}} \tag{3.9}$$

The solution of which is:

$$T_{\text{PVT}} = \left(T_{\text{amb}} - \frac{B}{A}\right)e^{-Ax} + \frac{B}{A} \tag{3.16}$$

where

$$A = -\frac{w}{\dot{V} \times \rho \times c_p}\left(\bar{h}_{\text{in}T}C1 + \bar{h}_{\text{in}}C3 - \left(\bar{h}_{\text{in}} + \bar{h}_{\text{in}T}\right)\right) \tag{3.17}$$

$$B = \frac{w}{\dot{V} \times \rho \times c_p}\left(\bar{h}_{\text{in}}C2 + \bar{h}_{\text{in}T}C4\right) \tag{3.18}$$

The convective heat transfer coefficient on the upper/outside surface of the PVT is dependent on the local wind speed (Vw) and is calculated from the correlation (3.19) by considering both the natural and forced convection components through the following relationship [12], in which the forced convection heat transfer coefficient $h_{\text{conv,forced}}$ is determined by Eq. (3.20) [16].

$$U_{\text{ext}} = \sqrt[3.5]{h_{\text{conv,forced}}{}^{3.5} + h_{\text{conv,natural}}{}^{3.5}} \tag{3.19}$$

$$h_{\text{conv,forced}} = 2.8 + 3.0 \times ws \tag{3.20}$$

The natural convection coefficient on the upper surface of the PVT is calculated according to the relationships of ASHRAE 2009 Fundamentals Handbook correlations for natural convection on a horizontal plate [14].

The internal convective heat transfer coefficient ($\bar{h}_{\text{in}}$) within the duct is dependent on the Reynolds number, which is different for laminar flow and turbulent flow. The heat transfer coefficient of the top half of the PVT channel ($\bar{h}_{\text{in}T}$) also includes the thermal resistance of the PV panels:(3.21)$\bar{h}_{\text{in}T} = \frac{1}{(1/h_{\text{in}})+R_{\text{pv}}}$

In this model, when the Reynolds number is lower than 2000, Eq. (3.22) is used to calculate the Nusselt number. Otherwise, the Dittus–Boelter relationship for turbulent flow as shown in Eq. (3.23) is used.

$$Nu_l = 7.541\left(1 - 2.61\text{AR} + 4.97\text{AR}^2 - 5.119\text{AR}^3 + 2.702\text{AR}^4 - 0.548\text{AR}^5\right) \tag{3.22}$$

$$Nu_t = 0.023Pr^n Re^{4/5} \tag{3.23}$$

where AR is the aspect ratio (height/width) of the channel, Pr is the Prandtl number of air and n is equal to 0.4 when the airflow is heated and 0.3 when the airflow is cooled.

The parameters needed to calculate the instantaneous intensity of solar radiation impinging on a tilted surface are summarised in Table 1.

In cases where only site data for global horizontal radiation is available, the horizontal surface radiation measurement can be used to estimate the diffuse and beam components. The coefficient R_b is used to define the ratio of beam radiation on the tilted surface to that on a horizontal surface.

$$R_b = \frac{\cos\theta}{\cos\theta_z} \tag{3.24}$$

where θ_z is the angle θ calculated for a horizontal surface as follows.

$$\cos\theta_z = \cos\varphi\cos\delta\cos\omega + \sin\varphi\sin\delta \tag{3.25}$$

The ratio between the diffused and beam radiation is calculated using the Orgill and Hollands correlation [16].

The effective emissivity of the solar panels may be calculated using empirical or semi-empirical correlations available in the literature [12,15]. Most of which are valid only for clear sky conditions [15], and while factors to take into account of cloudy conditions may be added [17]. The temperature of the sky in this study was calculated using the relationship for night-time clear sky radiation provided by Duffie and Beckman, as follows [16]:

$$T_{\text{sky}} = T_{\text{amb}} \times \left(0.711 + 0.0056T_{\text{dp}} + 0.000073\left(T_{\text{dp}}{}^2\right) + 0.013\cos(15t)\right)^{1/4} \tag{3.26}$$

where the units for T_{sky} and T_{amb} are Kelvin, for T_{dp} degrees Celsius, and t is the time of day in hours.

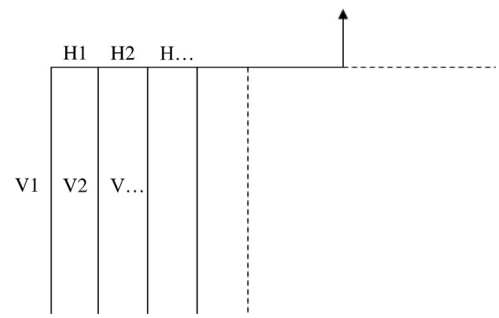

Fig. 7. Air flow resistance network showing flow elements/resistances for flow branches connected to the air collection manifold. V1, V2, etc. represent PVT ducts and H1, H2, etc. represent manifold sections.

Cloudiness has an effect on the incident radiation which can be expressed by the factor C as shown in Eq. (3.27) [17,18] and the effective emissivity of the sky is given by (3.28).

$$C = \left(1 + 0.00224n + 0.0035n^2 + 0.00028n^3\right) \tag{3.27}$$

$$\varepsilon_{\text{sky,cloudy}} = C\varepsilon_{\text{sky,clear}} \tag{3.28}$$

The linearized radiation heat transfer coefficient between the sky and the PV panels is defined as (3.29). Using the same methodology the radiation coefficient between the top plate and bottom plate of the PVT channel is derived as Eq. (3.30).

$$h_{r1} = \alpha\sigma\left(T_{\text{top}}{}^2 + T_{\text{sky}}{}^2\right)\left(T_{\text{top}} + T_{\text{sky}}\right) \tag{3.29}$$

$$h_{r2} = \alpha\sigma\left(T_{\text{top}}{}^2 + T_{\text{bot}}{}^2\right)\left(T_{\text{top}} + T_{\text{bot}}\right) \tag{3.30}$$

where σ is the Boltzmann constant, α is the absorptivity of the metal flashing, T_{top} is the sky temperature, and T_{top} is the temperature of the top plate of the PVT channel, which is calculated iteratively.

3.2. Airflow model

To optimize the airflow rate through a PVT collector it is necessary to take into account the fan power required to circulate the air through the PVT and ductwork system. Firstly, the air velocity through the PVT channels, and other ductwork, and the associated pressure drops need to be calculated. To calculate these parameters an equivalent hydraulic resistance network was analysed (Fig. 7).

This analysis was important in choosing the optimal number and size of the PVT channels and in optimising the geometry of the manifold, since a uniform air flow velocity through the PVT channels is important to maximise the overall efficiency.

One of the assumptions made in this model is that, since the channels are uniformly distributed across the intake manifold, the flows will be symmetrical, and it is therefore necessary to model only one half of the system. Major and minor losses are calculated for each of the sections of the network by first assuming the flow in the first channel it is then possible to calculate the pressure at the manifold point where the second channel is connected and therefore calculate the flow in the second channel. Repeating the process the pressure drop of the whole network for a given airflow rate, and the flow distribution across the network can be obtained. The pressure–airflow curve for this particular system can then be determined. Since both sides of the roof are equal and symmetrical, the curve of just one side can be generated, assuming that each side of the PVT has half of the total airflow rate. The power necessary to ideally circulate the air through the system can then be calculated by the following equation:

$$P_{\text{id}} = \Delta p\Delta\dot{V} \tag{3.31}$$

where Δp is the total pressure drop and $\dot{V}$ is the total airflow rate.

Table 1
Values and governing equations used to determine the values of major parameters.

Parameters	Values and governing equations used
Albedo	0.2
Hour angle	$\omega = 2\pi(stn - 12) \times 15/360$
Declination	$d = 23.45 \times \sin\left(360 \times (284 + doy)/365\right) \times 2\pi/360$
The angle θ between the normal to the inclined plane and the beam radiation	$\cos\theta = \sin d \sin\varphi \cos\beta - \sin\delta \cos\varphi \sin\beta \cos\gamma + \cos\delta \cos\varphi \cos\beta \cos\omega + \cos\delta \sin\varphi \sin\beta \cos\gamma \cos\omega + \cos\delta \sin\beta \sin\gamma \sin\omega$
The radiation on an inclined surface	$G_{\text{inclined}} = \text{dnr}\cos\theta + \left(\text{dhr}\left(1 + \cos\beta\right)/2\right) + 0.2(\text{ghr} + \text{dhr})\left(1 - \cos\beta\right)/2$

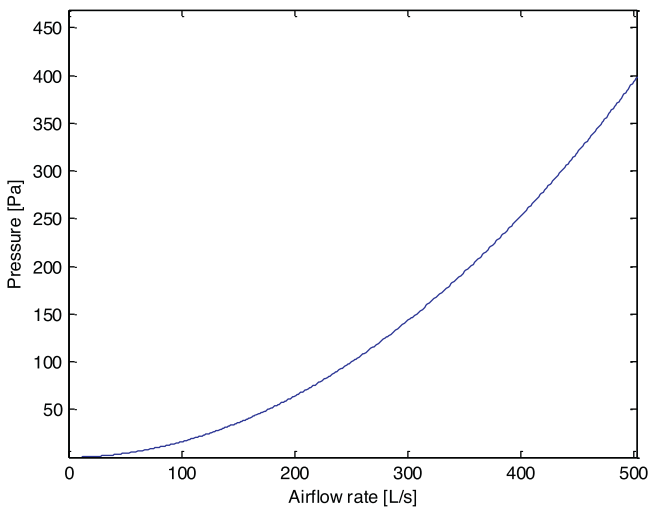

Fig. 8. Pressure–airflow characteristic of the 'Illawarra Flame' Solar Decathlon house PVT collector.

With a cubic interpolation of Eq. (3.32), a relationship that can be used later for optimization purposes that can include the overall efficiency of the fan.

$$P_{e,\text{cons}} = \frac{P_{\text{id}}}{\eta} = \gamma_{\text{PVT}} \dot{V}^3 \tag{3.32}$$

The pressure–airflow rate curve calculated for the Solar Decathlon house PVT system is shown in Fig. 8.

3.3. PV electrical efficiency

Drawing air underneath the solar panels has the benefit of reducing the panel temperature as described by [18] and a reduction in the temperature of the solar panels increases their electrical conversion efficiency. This benefit can be quantified using the temperature coefficient of the solar panels, β. Using the thermal model developed for the air stream, presented in Section 3.1, the temperature profile of the top sheet of the PVT collector (T_{top}) can be calculated. The efficiency is therefore given by the following equation:

$$\eta_e = \eta_{e\text{-ref}} \times \left(1 - \beta \times \left(T_{\text{top}} - 25\right)\right) \tag{3.33}$$

where $\eta_{e\text{-ref}}$ is the efficiency under standard test conditions.

4. Analytical model of the PCM thermal storage unit

The PCM thermal storage unit in the Solar Decathlon house was designed to exchange heat between the PCM and the air. The practical PCM thermal storage unit consisted of 120 PlusIce™ salt hydrate PCM 'bricks' [13], with a nominal phase change temperature of 22 °C, placed in twenty rows of six so as to create channels for the air to flow through. The channels were 3 m long and the latent heat capacity of the whole unit was 20 kW h, sufficient for approximately two days of heating or cooling demand of the house.

4.1. Thermal model

A number of assumptions were applied so as to facilitate derivation of an analytical solution to reduce the computational load of the controller. These assumptions were:

- the temperature of the PCM is uniform along the entire length of the heat exchanger at any given time (lumped mass approximation);
- the PCM material changes phase at a specific temperature (with no temperature 'glide');
- the material encapsulating the PCM brick has the same thermal conductivity as that of the PCM material per se. Note that in the Solar Decathlon house thermal store, the encapsulation was made of high-density polyethylene (HDPE) which had a very similar thermal conductivity to that of the PCM.

Given the assumptions above the air temperature as a function of distance along each channel is given by:

$$T_{\text{PCM},m} = T_{\text{pcm}} - \left(T_{\text{pcm}} - T_{\text{PCM},i}\right) e^{\left(-P\bar{h}x/(\dot{V} \times \rho \times c_p)\right)} \tag{4.1}$$

where $T_{\text{PCM},m}$ is the average temperature of the air at a distance x along the channel, T_{pcm} is the surface temperature of the channel (assumed equal to the PCM temperature), $T_{\text{PCM},o}$ is the inlet air temperature, P is the perimeter of the channel, $\bar{h}$ is the average internal convective heat transfer coefficient.

Similarly, the outlet temperature at the length l can be determined by the following equation:

$$T_{\text{PCM},o} = T_{\text{pcm}} - \left(T_{\text{pcm}} - \left(T_{\text{pcm}} - T_{\text{PCM},i}\right)\right) e^{\left(-P\bar{h}l/(\dot{V} \times \rho \times c_p)\right)} \tag{4.2}$$

The average internal convective heat transfer coefficient can be calculated using the Nusselt number definition.

$$\bar{h} = \frac{k\overline{Nu}}{D_h} \tag{4.3}$$

The correlations to evaluate the average Nusselt number for a fully developed laminar flow in a rectangular duct are the same as those presented in (3.22) and (3.23).

To include the thermal resistance of the wall and PCM material in the modelling, it is possible to rewrite the equation with the total heat transfer coefficient (U_{tot}).

$$R_{\text{conv}} = \frac{1}{\bar{h}} \tag{4.4}$$

$$R_{\text{cond}} = \frac{1}{U_{\text{wall+PCM}}} \tag{4.5}$$

$$U_{\text{tot}} = \frac{1}{R_{\text{cond}} + R_{\text{conv}}} \tag{4.6}$$

This coefficient in Eq. (4.6) has to be substituted by Eqs. (4.1) and (4.2) to $\bar{h}$.

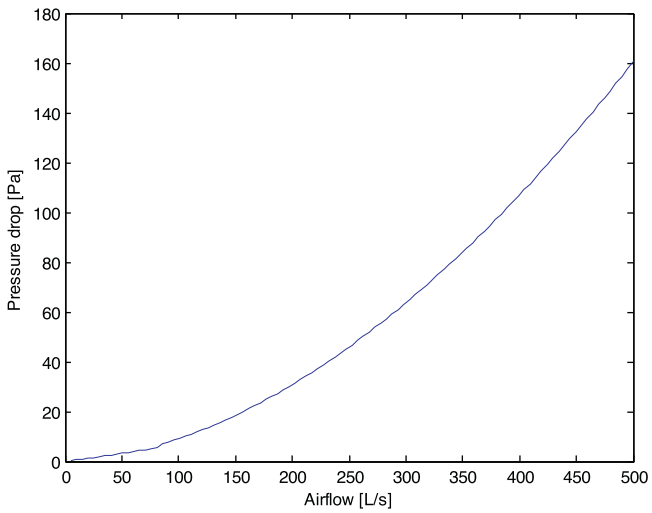

Fig. 9. Pressure drop-airflow through the PCM thermal storage unit.

The total heat transfer can be calculated as follows:

$$Q = \dot{m}c_p\,(T_{\text{in}} - T_{\text{out}}) \tag{4.7}$$

4.2. Mechanical analysis

As for the PVT collector it is necessary to take into account the power required to drive the air through the PCM thermal store. The material in contact with the air in this case is plastic, with a roughness ε [14]. Fig. 9 shows the pressure–airflow curve. Following the same methodology presented in Section 3.2, including the efficiency of the fan, the resulting 3rd order fit for the power consumption is of the same form:

$$P_{e,\text{cons}} = \gamma_{\text{PCM}}\dot{V}^3 \tag{4.8}$$

This relationship will be used later for system optimization. The pressure–airflow rate curve of the PCM thermal energy storage unit implemented in the Solar Decathlon house is presented in Fig. 9.

5. Field tests and validation

In this section the results from both experiments and simulations are presented. The PVT and PCM models were implemented in Matlab and the response of the two sided collector was simulated. For some of these simulations, Sydney IWEC (International Weather for Energy Calculations) weather data was used.

The models were then validated using the experimental data collected in both Datong, China, during the Solar Decathlon China competition and later at the University of Wollongong following the return of the Illawarra Flame House to Australia.

5.1. Experimental facilities

The PVT tests were first carried out during August 2013 in Datong, China, and then in Wollongong, Australia, from June 2014 onwards. The PVT collector, integrated with the HVAC system of the house, was controlled and monitored through a Clipsal C-Bus building management system. All the relevant parameters were monitored and logged using a JACE-6 controller at a one-minute sample rate.

The weather conditions, including ambient temperature, solar radiation and wind speed and direction, were monitored using a Davis Vantage Pro II Weather station and integrated through an RS232 connection to the C-Bus and JACE control units. Airflow was monitored using Siemens QVM62.1 air velocity sensors, located one third of the duct diameter from the duct centreline. These sensors had a stated accuracy of ±0.2 m/s + 3% of measured values. Temperatures in the ductwork were measured using Clipsal C-Bus Digital Temperature Sensor Units 5104DTSI with a stated accuracy of ±0.5 °C in the temperature range of −10–80 °C.

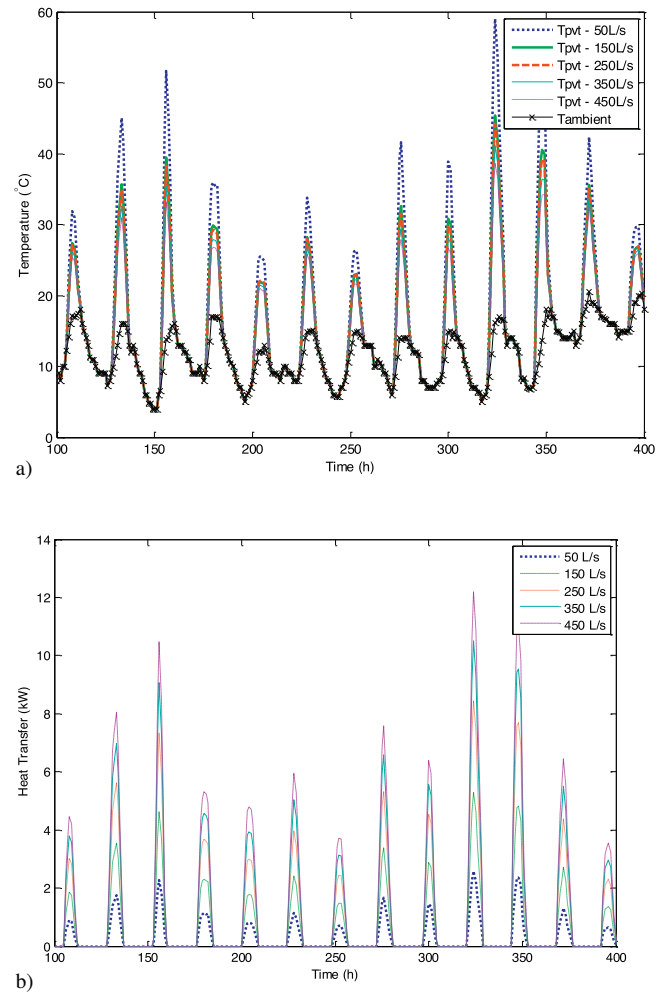

Fig. 10. Temperature difference and heat transfer from the PVT collector under different air flow rates for July, Sydney, IWEC weather conditions.

5.2. Validation of the PVT thermal model

The simulated PVT outlet air temperatures and the heat transfer rates under various air flow rates as well as the ambient air temperature, based on the IWEC July weather data of Sydney, are shown in Fig. 10.

It can be seen that an increase in the airflow rate in the PVT collectors led to a decrease in the PVT outlet temperature and hence an increase in both the total heat transfer to the air and the thermal efficiency of the system. Simulations were also performed for the summer cooling case, where the sky temperature was calculated using (3.27). Using the Sydney IWEC weather data and considering the cloudiness factor, the total cooling was calculated to reach 1.5 kW when the airflow rate is 300 L/s.

The global horizontal radiation, ambient temperature, predicted PVT outlet temperatures and measured PVT outlet temperatures in Wollongong, Australia, for June 2014 are shown in Fig. 11.

During these experimental tests the PVT airflow rate was maintained at 350 L/s. It can be seen that a very good agreement between the predicted PVT outlet temperatures and measured values was

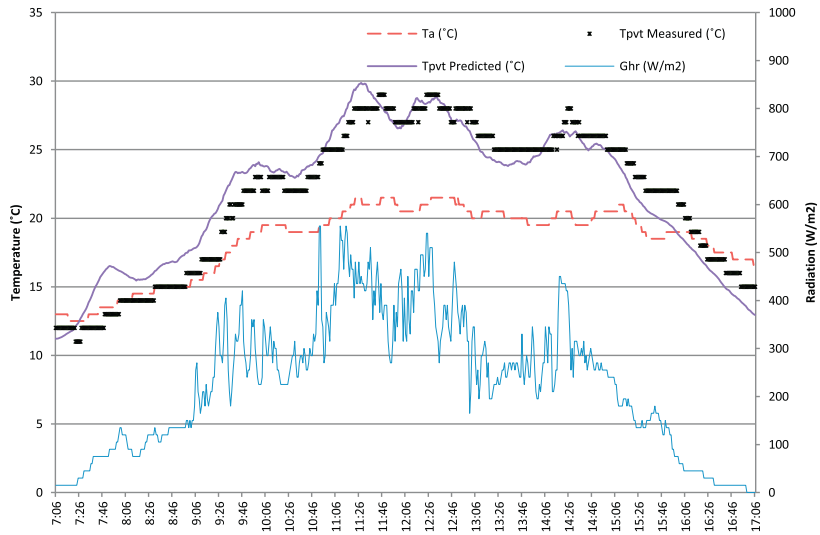

Fig. 11. Comparison of the predicted PVT air outlet temperatures with the measured values (June 2014, Wollongong, Australia).

achieved. It is also seen that the experimental results lag the simulations by short time, less than five minutes, since the quasi-steady state thermal model of the PVT does not account for the relatively small thermal mass of the PVT collector.

A scatter plot of the predicted versus measured PVT outlet temperatures is shown in Fig. 12, which provides substantive evidence that the simulations matched experiments with a linear regression coefficient $b = 0.9911$ and $R^2_{adj} = 0.9122$.

This is considered to be a good result noting that the scatter in the data was in part due to the non-controlled and transient environment and that the data acquisition system has a course resolution on temperature due to the limitations of the residential building management system employed. In addition, the assumed negligible PVT collector thermal mass used in the thermal model also contributed somewhat to the scatter in the data.

The measured total electrical energy generated from the PVT roof, and that modelled as generated from both the north and south elevations of the PVT collector (viz Fig. 5, using the published performance data of the CIGS solar panels and global insolation measured during field tests, are compared in Fig. 13.

A scatter plot of the predicted versus measured PVT electrical generation is shown in Fig. 14, with a linear regression coefficient $b = 0.9947$, intercept $a = -137$ and $R^2_{adj} = 0.8904$. This indicates a relatively good agreement between the two sets of data, with the model slightly over-predicting the electrical generation.

The thermal efficiency, electrical efficiency and total efficiency of the PVT collector under the experimental tests at Datong, during August 2013, are shown in Fig. 15.

It can be seen that the overall electrical efficiency of the PVT collector is relatively constant (i.e. ~8.2%) and consistent with the expected efficiency, considering that the published PV conversion efficiency was stated as 11.2% and the inverter efficiency taken to be 95%. Even with a relatively low air flow (i.e. 160–170 L/s), the heat transfer to the air was as high as 4.0 kW, equating to a thermal efficiency of around 9.0%. The effect of extracting thermal energy from the PV panels was to increase the overall system efficiency to around 17%.

5.3. Experimental validation of the PCM thermal model

The results of simulations of the performance of the PCM thermal storage unit are shown in Fig. 16. The simulated air temperature profiles along the length of the PCM thermal storage unit under various airflow rates are shown as a function of distance from the

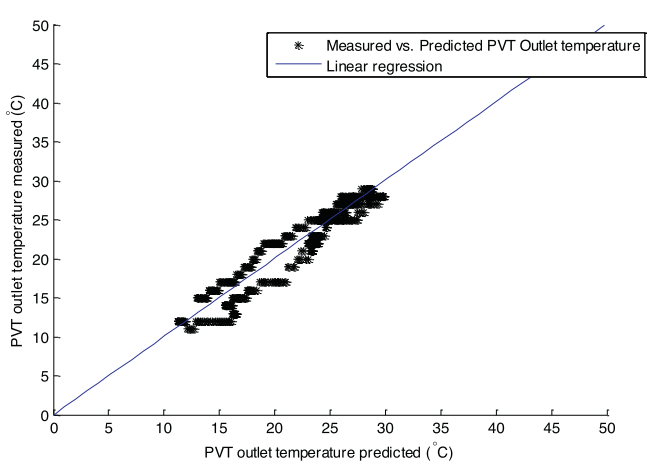

Fig. 12. A scatter plot of measured and predicted PVT air outlet temperature data (June 2014, Wollongong, Australia).

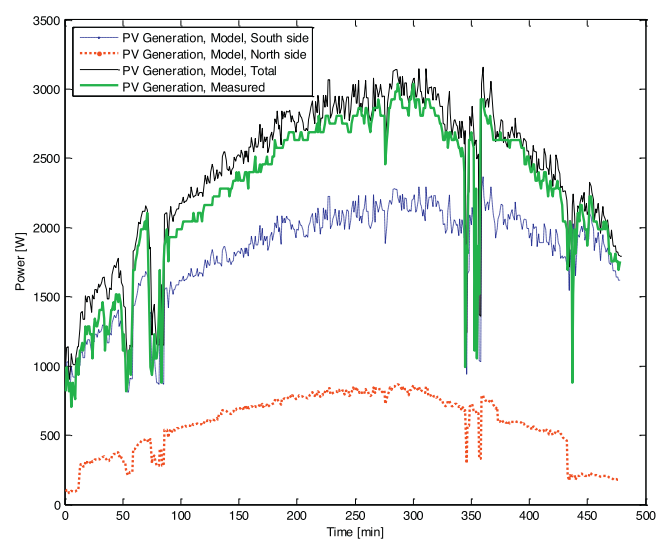

Fig. 13. Predicted and measured PV electrical energy generation as a function of time (experiments conducted at Datong, China, during August 2013).

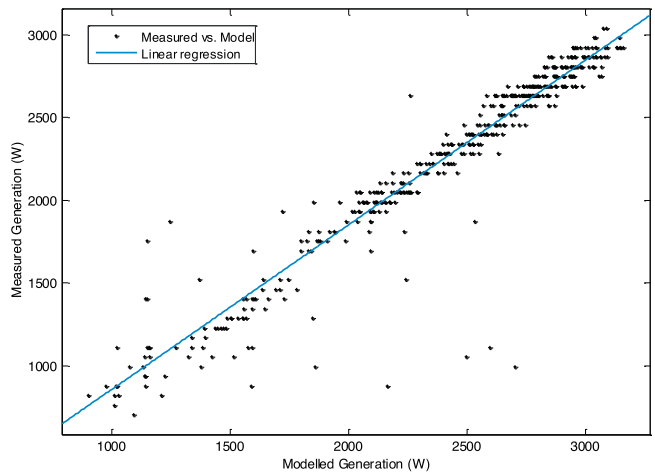

Fig. 14. A scatter plot of measured and predicted PVT electrical generation.

inlet. As expected it was found that increasing the airflow rate led to higher heat transfer rates and higher outlet air temperature.

Experimental tests on the PCM thermal storage unit were carried out on a laboratory-scale test rig at the University of Wollongong, which was essentially a replica of the Illawarra Flame House PCM thermal store system with the same length of 3 m, but with a reduced number of channels. The total mass of FlatIce™ PCM in the lab-scale rig was 138 kg, as compared to 693 kg in the Solar Decathlon house per se. The same equipment was used to measure and log the temperature and air flow data as that for the PVT tests described above, and a sample rate of 15s was employed for the transient heating and cooling tests on the PCM store.

The modelled and experimentally determined total UA values for the heat exchanger under different flow rates are shown in Fig. 17, where UA values for the experimental tests were found by dividing the total heat exchange of the fluid by the log-mean temperature difference (LMTD).

6. Optimisation of operating modes

6.1. PCM unit charging with PVT

The models developed can be used for the optimisation of the various operating modes. For example the optimization of the PCM

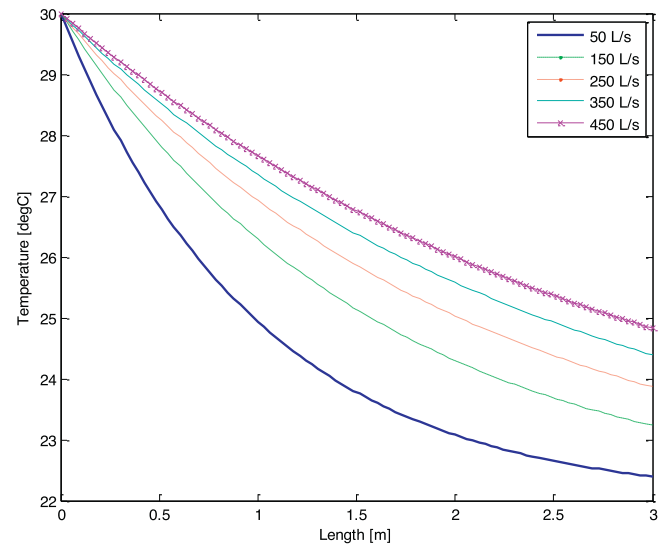

Fig. 16. Modelled air temperature profile along the length of the PCM thermal storage unit under different airflow rates.

charging mode requires the control system to choose an optimal airflow rate that can maximise the benefit in terms of the heat stored in the PCM unit and how much energy is being used by the fan. In this study, a cost function as expressed in Eq. (6.1) is used to maximize the amount of heat stored, considering that this would lead to certain electrical power consumption and an increase in the electrical generation that has to be somehow related to the heat transfer.

$$C(\dot{m}) = P_{\text{th}}(\dot{m}) + \alpha_c \left(\Delta P_{e,\text{gen}}(\dot{m}) - P_{e,\text{cons}}(\dot{m})\right) \tag{6.1}$$

$$P_{\text{th}}(\dot{m}) = \rho \dot{V} c_p \left(T_{\text{PVT}}(\dot{m}) - T_{\text{PCM},o}(\dot{m})\right) \tag{6.2}$$

where $\dot{V}$ is the flow rate of air flowing in the system, c_p is the air specific heat capacity at 20 °C, ρ is the density, P_{th} is the heat transfer rate into the PCM thermal storage unit as defined in Eq. (3.2), $\Delta P_{e,\text{gen}}$ is the increase in electrical generation due to the cooling of the solar panels, $\Delta P_{e,\text{cons}}$ is the power consumption of the fan to move the air into the system, T_{pvt} and $T_{\text{pcm},o}$ are, respectively, the PVT outlet temperature (which corresponds to the inlet temperature of the

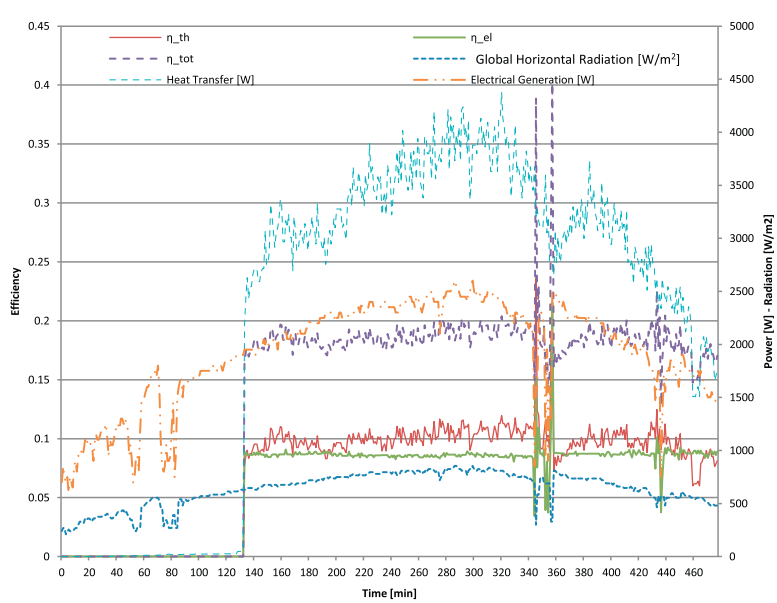

Fig. 15. PVT efficiency as measured during testing August 2013 at Datong, China (η_th, η_el, η_tot are the PVT thermal, electrical and total efficiency, respectively).

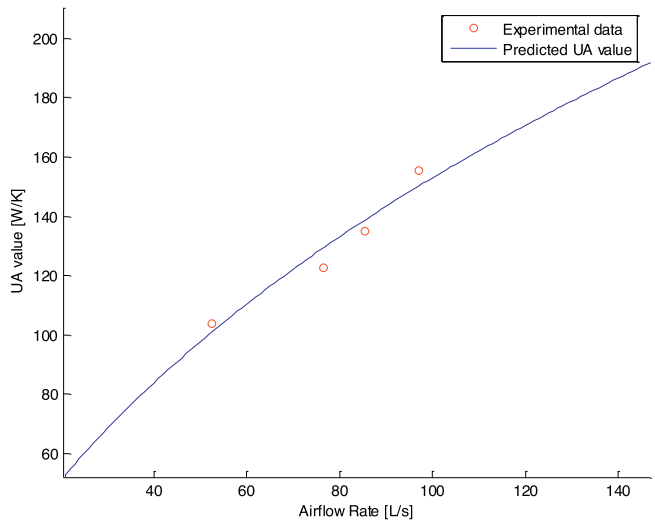

Fig. 17. Comparison between modelled UA values (line) and experimental results (circles) of the laboratory-scale PCM thermal storage unit.

PCM if the thermal losses in the ducting can be considered negligible), α_c is a weighting factor for the electrical energy to increase its importance relatively to the thermal energy. The choice of this factor might be different from case to case, depending on the design objectives.

The simulated heat transfer, increased electrical generation of the PV panels and the electrical energy used by the fans are presented in Fig. 18. This simulation was based on a single-sided PVT system in a winter heating scenario with the ambient temperature of 18 °C, indoor temperature of 25 °C, wind speed of 1 m/s. The radiation level on the tilted surface was 750 W/m^2.

The heat transfer into the PCM unit can then be correlated to the electrical power consumption of the fan and the increased electrical generation of the PV panels. Discontinuities in Fig. 18 due to the changes in the heat transfer coefficient calculation between laminar flow and turbulent flow have been smoothed.

It is then possible to obtain the cost function curves (Eq. (6.1)) and identify the optimal airflow rate which corresponds to the maximum of the cost function under the different weather conditions (Fig. 19). The discontinuities in this case due to the changes in the

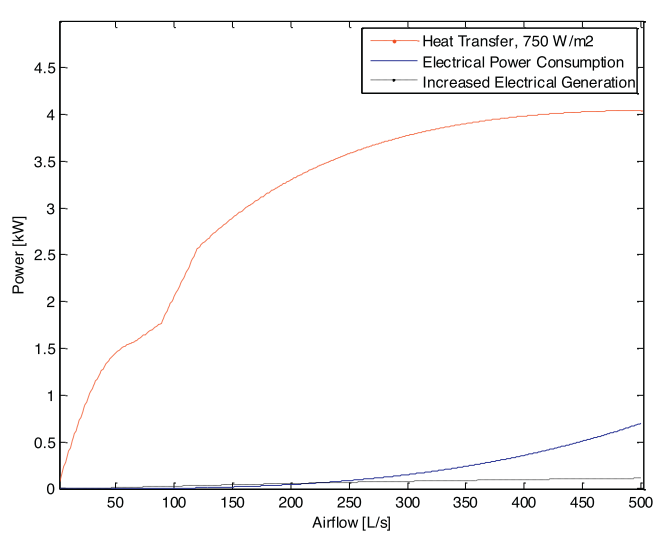

Fig. 18. Heat transfer, increased electrical generation and electrical power consumption.

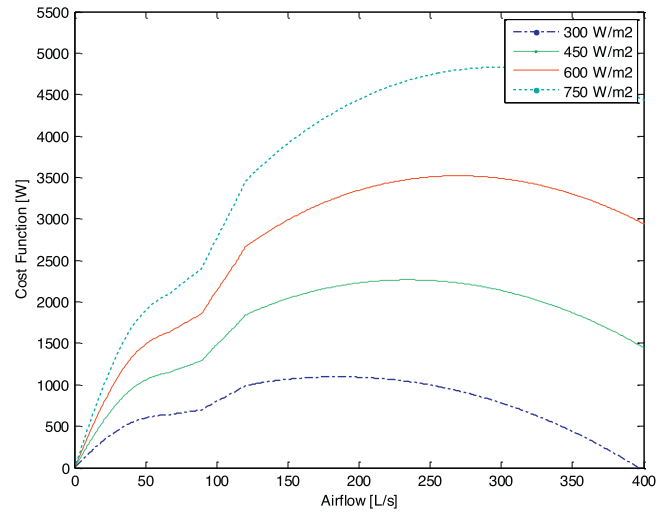

Fig. 19. Evaluation of the cost function under different radiation levels.

heat transfer coefficient calculation between laminar and turbulent flow have also been smoothed.

6.2. Conditioning house with Direct PVT air supply

The optimisation of the Direct PVT supply mode is very similar to that of the optimisation of the PCM charging mode, using the same cost function as presented in Eq. (6.1). The calculation of the heating generated for the house is calculated as the following equation:

$$P_{\text{th}}(\dot{m}) = \rho \dot{V} c_p \left(T_{\text{pvt}}(\dot{m}) - T_{\text{house}}\right) \tag{6.3}$$

where T_{house} is the average temperature of the house.

6.3. Conditioning house with PCM Discharging air supply

Similar to the PCM charging mode, the performance of the PCM discharging mode is highly dependent on the inlet temperature of the PCM thermal storage unit. In this operating mode, the inlet temperature is a mixture of the return air from the house and the fresh air from ambient. The ratio between the two air streams is dependent on the decisions taken at the design stage. Since there is no electrical generation involved, the optimisation of this working mode is to maximise the cost function below.

$$C(\dot{m}) = P_{\text{th}}(\dot{m}) - \alpha_c \left(P_{e,\text{cons}}(\dot{m})\right) \tag{6.4}$$

where P_{th} is the heat discharged from the PCM unit, defined as the following equation:

$$P_{\text{th}}(\dot{m}) = \rho \dot{V} c_p \left(T_{\text{PCM},o}(\dot{m}) - T_{\text{PCM},i}(\dot{m})\right) \tag{6.5}$$

where $T_{\text{pcm},i}$ is the inlet temperature of the PCM unit, which is a mixture of the return air from the house and fresh air.

7. Conclusions

This paper outlined a modelling methodology for the thermal, hydraulic and electrical characteristics of a photovoltaic–thermal (PVT) system, and the thermal and hydraulic behaviour of an integrate phase change material (PCM) thermal storage unit. This methodology is efficient and can be readily implemented in practice through the logic of an off-the-shelf residential building management system. In particular, the analytical solutions of the thermal models of the PVT and PCM systems guarantee the possibility of using these models for operational optimization with minimal computational effort.

The experimental field work and laboratory tests using a full-scale Solar Decathlon house and a laboratory-scale PCM thermal store test rig showed that this modelling methodology can provide sufficient accuracy for control purposes, despite its elegant simplicity. A simple optimisation methodology of the operating modes that involve these components is also presented.

Future work will be focused on the utilization of these component models for system optimization of the operation of the HVAC system incorporating a PVT collector, PCM thermal store, and conventional heat pump and air handling unit.

Acknowledgements

The authors would like to thank members of Team UOW and BlueScope for their assistance in the development of the PVT system, and Dr Josh Wall and colleagues of the Commonwealth Scientific and Industrial Research Organization (CSIRO) for their valuable advice and support in sourcing control and data acquisition equipment.

References

[1] Z. Ma, P. Cooper, D. Daly, L. Ledo, Existing building retrofits: methodology and state-of-the-art, Energy Build. 55 (2012) 889–902.
[2] R. Baetens, B.P. Jelle, A. Gustavsen, Phase change materials for building applications: a state-of-the-art review, Energy Build. 42 (2010) 1361–1368.
[3] W. Lin, Z. Ma, M.I. Sohel, P. Cooper, Development and evaluation of a ceiling ventilation system enhanced by solar photovoltaic thermal collectors and phase change materials, Energy Convers. Manage. 88 (2014) 218–230.
[4] J.J. Jurinak, S.I. Abdel-Kalik, On the performance of air-based solar heating systems utilizing phase–change energy storage, Energy 4 (1979) 503–522.
[5] J.J. Jurinak, S.I. Abdel-Kalik, Properties optimization for phase-change energy storage in air based solar heating systems, Solar Energy 21 (1978) 377–383.
[6] J.J. Jurinak, S.I. Abdel-Kalik, Sizing phase change energy storage units for air-based solar heating systems, Solar Energy 22 (1979) 355–359.
[7] M. Pomianowskia, P. Heiselberga, Y. Zhang, Review of thermal energy storage technologies based on PCM application in buildings, Energy Build. 67 (2013) 56–69.
[8] N. Zhu, S. Wang, X. Xu, Z. Ma, A simplified dynamic model of building structures integrated with shaped-stabilized phase change materials, Int. J. Therm. Sci. 49 (2010) 1722–1731.
[9] Y. Chen, A.K. Athienitis, K. Galal, Modeling, Design and thermal performance of a BIPV/T system thermally coupled with a ventilated concrete slab in a low energy solar house: Part 1, BIPV/T system and house energy concept, Solar Energy 84 (2010) 1892–1907.
[10] Y. Chen, A.K. Athienitis, K. Galal, Modeling, design and thermal performance of a BIPV/T system thermally coupled with a ventilated concrete slab in a low energy solar house: Part 2, ventilated concrete slab, Solar Energy 84 (2010) 1908–1919.
[11] S. Pantic, L. Candanedo, A.K. Athienitis, Modeling of energy performance of a house with three configurations of building-integrated photovoltaic/thermal systems, Energy Build. 42 (2010) 1779–1789.
[12] Ursula Eicker, Antoine Dalibard, Photovoltaic–thermal collectors for night radiative cooling of buildings, Solar Energy 85 (2011) 1322–1335.
[13] PCM Products. Available from: www.pcmproducts.net (accessed 03.03.15).
[14] ASHRAE handbook – fundamentals (SI Edition), in: Heat Transfer, American Society of Heating, Refrigerating and Air-Conditioning Engineers, Inc., Atlanta, GA, 2009, pp. 4.1–4.21 (Chapter 4).
[15] P. Berdahl, R. Fromberg, The thermal radiance of clear skies, Solar Energy 29 (1982) 299–314.
[16] J.A. Duffie, W.A. Beckman, Solar Engineering of Thermal Processes, 4th ed., John Wiley & Sons, Somerset, NJ, USA, 2013, pp. 43–170, ProQuest ebrary. Web. 2 March 2015.
[17] G. Mihalakakou, A. Ferrante, J.O. Lewis, The cooling potential of a metallic nocturnal radiator, Energy Build. 28 (1998) 251–256.
[18] H.S. Bagiorga, G. Mihalakakou, Experimental and theoretical investigation of a nocturnal radiator for space cooling, Renewable Energy 33 (2008) 1220–1227.